XPS and EELS Characterization of Mn_2SiO_4, $MnSiO_3$ and $MnAl_2O_4$

A.P. Grosvenor[1], E.M. Bellhouse[2], A. Korinek[3], M. Bugnet[3] and J.R. McDermid[4*]

[1]Department of Chemistry, University of Saskatchewan, Saskatoon, SK, Canada, S7N 5C9
Phone: (306) 966-4660
Email: andrew.grosvenor@usask.ca

[2] Global R & D – Hamilton, ArcelorMittal Dofasco, 1330 Burlington St. E, Hamilton, ON, Canada, L8N 3J5
Phone: (905) 548-7200 ext. 3554
Email: erika.bellhouse@arcelormittal.com

[3]Canadian Centre for Electron Microscopy, Brockhouse Institute for Materials Research, McMaster University, 1280 Main St. W., Hamilton, ON, Canada, L8S 4M1
Phone: (905) 525-9140 x24071
Email: korinek@mcmaster.ca
Email: bugnetm@mcmaster.ca

[4*]Steel Research Centre, McMaster University, 1280 Main St. W., Hamilton, ON, Canada, L8S 4M1
Phone: (905) 525-9140 x27476
Email: mcdermid@mcmaster.ca (corresponding author)

Abstract

X-ray Photoelectron Spectroscopy (XPS) and Electron Energy Loss Spectroscopy (EELS) are strong candidate techniques for characterizing steel surfaces and substrate-coating interfaces when investigating the selective oxidation and reactive wetting of advanced high strength steels (AHSS) during the continuous galvanizing process. However, unambiguous identification of ternary oxides such as Mn_2SiO_4, $MnSiO_3$, and $MnAl_2O_4$ by XPS or EELS, which can play a significant role in substrate reactive wetting, is difficult due to the lack of fully characterised standards in the literature. To resolve this issue, samples of Mn_2SiO_4, $MnSiO_3$ and $MnAl_2O_4$

were synthesized and characterized by XPS and EELS. The unique features of the XPS and EELS spectra for the Mn_2SiO_4, $MnSiO_3$ and $MnAl_2O_4$ standards were successfully derived, thereby allowing investigators to fully differentiate and identify these oxides at the surface and subsurface of Mn, Si and Al alloyed AHSS using these techniques.

Keywords: X-ray Photoelectron Spectroscopy, Electron Energy Loss Spectroscopy, selective oxidation, manganese silicates, manganese aluminates

1 Introduction

In order to meet Corporate Average Fuel Economy (CAFE) requirements, automobile manufacturers are increasing their use of advanced high strength steels (AHSS) such as dual phase steels (DP) and transformation induced plasticity (TRIP) steels and and are demanding third generation AHSS (3G AHSS) steels such as quench and partition (Q&P) and so-called medium manganese 3G AHSS. These steels employ significant alloying levels of manganese and tend to have significant alloying levels of silicon and\or aluminum [1-6]. These alloying elements form selective oxides on the steel surface during annealing prior to continuous galvanizing, which can result in poor reactive wetting during galvanizing and bare spot defects in the zinc coating. Many studies have focused on identifying these selective oxides and relating them to the reactive wetting behaviour in the metallic coating bath [1-3,7- 17]. However, accurate identification of these compounds has been challenging due to a lack of high resolution X-ray photoelectron spectroscopy (XPS) and electron energy loss spectroscopy (EELS) data on the ternary oxides $MnSiO_3$, Mn_2SiO_4 and $MnAl_2O_4$. Both XPS and EELS spectra are required as XPS is suitable for chemical analysis of the steel surface after selective oxidation and prior to metallic coating and EELS is suitable for studying the steel-coating interface, which may have

oxides remaining at the interface after metallic coating, or within the bulk steel itself due to selective internal oxidation [1-3,8,9,12,13,15-17]. The use of these surface (XPS) and near-surface sensitive (EELS) techniques is necessary to identify these oxides since neither technique requires that the oxides be highly ordered to study them, as is required when using X-ray diffraction for quantitative phase analysis.

The XPS binding energies for elemental Mn, Si and Al and the binary oxides MnO, SiO_2 and Al_2O_3 are readily available in the literature [18-22]. However, limited XPS binding energy data are available for the ternary oxides Mn_2SiO_4 and $MnAl_2O_4$, as summarized in List of **Figures**

Figure 1: Powder X-ray diffraction patterns from (a) MnAl2O4, (b) MnSiO3, and (c) Mn2SiO4 collected using a Cu Kα1 X-ray source. The collected diffraction patterns are compared to the calculated diffraction patterns determined using the known structures of the materials [29]. The major peaks from the impurity phases are marked with an asterisk in the powder XRD patterns.

Figure 2: Background subtracted Mn $2p3_{/2}$ high resolution XPS spectra from (a) MnAl2O4, (b) MnSiO3, and (c) Mn2SiO4. The background was removed using a Shirley-type background and the spectra were fitted using multiplet peaks and a shake-up satellite peak using the method described in [21]. The resulting fit is indicated by a grey line.

Figure 3: Crystal structures of (a) MnAl2O4, (b) MnSiO3, and (c) Mn2SiO4. Mn-O polyhedra are shown in green, Si-O polyhedral are shown in purple, and Al-O polyhedral are presented in blue. Mn is 4-coordinate in MnAl2O4, whereas distorted 6- and 7-coordinate Mn ions are present in MnSiO3, while Mn occupies distorted octahedral environments in Mn2SiO4.

Figure 4: Background subtracted O 1s high resolution XPS spectra from (a) MnAl2O4, (b) MnSiO3, and (c) Mn2SiO4. The spectra were fitted by three component peaks to adequately reproduce each spectrum. The lowest energy peak represents O ions bound to Mn/Al/Si while the highest energy peaks likely represents adsorbed water and hydroxide functional groups [36].

Figure 5: Background subtracted high resolution Al 2p XPS spectrum from (a) MnAl2O4 and high resolution Si 2p XPS spectra from (b) MnSiO3 and (c) Mn2SiO4. Each spectrum has been fitted by a set of spin-orbit split $2p3_{/2}$ (low energy) and $2p1_{/2}$ (high energy) peaks having a 2:1 intensity ratio.

Figure 6: Mn-L2,3 edge electron energy loss spectra. The spectra were aligned to the most intense fine structure of the L3 edge at approximately 640 eV. The spectra were normalized to have an equal intensity of the L3 edge and were offset for clarity.

Figure 7: O-K edge electron energy loss spectra. The alignment and normalization of the spectra were performed with respect to the most intense fine structure of the Mn-L3 edge (Figure 6) and the spectra were offset for clarity.

List of Tables

Table 1 []. No XPS binding energy data could be found for $MnSiO_3$ when present as a pure species. Limited binding energy data are also available for Mn_2SiO_4 and $MnSiO_3$ when present with other species [24-27]. Thus, the purpose of the present contribution is to provide these spectra using $MnSiO_3$, Mn_2SiO_4 and $MnAl_2O_4$ standards prepared by the ceramic method.

2 Experimental Methods

2.1 Synthesis

All materials examined were synthesized using the ceramic method. $MnAl_2O_4$ was synthesized by heating a stoichiometric mixture of MnO (Alfa Aesar; 99.99%) and Al_2O_3 (Aldrich; 98% minimum) at 1000°C for a total of approximately six days before being cooled to room temperature over a period of approximately five hours. The synthesis of $MnAl_2O_4$ was performed under the cover of flowing forming gas (5% H_2, 95% N_2 (vol%)). $MnSiO_3$ and Mn_2SiO_4 were synthesized by heating stoichiometric quantities of MnO and SiO_2 (Alfa Aesar; 99.99%) in alumina crucibles enclosed in evacuated fused silica tubes at 1050°C for approximately 4 days. After the initial reaction, the purity of the $MnSiO_3$ was improved by adding approximately 5% (by mass) SiO_2 to the mixture before firing again at 1050°C under the same conditions described above for approximately two days [28]. The $MnSiO_3$ and Mn_2SiO_4 materials were quench cooled in air after the final firing.

The phase purity of the synthesized materials was determined using a PANalytical Empyrean powder X-ray diffractometer and a Cu $K_{\alpha 1}$ X-ray source. The phase purity of the materials was

determined by comparing the experimentally collected patterns to patterns that were calculated based on the structure of the target materials, the precursor oxides, and other related oxides. All materials were confirmed to have a phase purity of greater than 90% when compared to the established diffraction patterns of these materials [29]. It was unlikely that the minor impurities present affected the spectral results to be presented below owing to the resolution of the XPS and EELS spectra.

2.2 XPS data acquisition

XPS measurements were performed using a Kratos AXIS Ultra spectrometer fitted with a monochromatic Al Kα (1486.7 eV) X-ray source located at Surface Science Western, the University of Western Ontario. The area analyzed was approximately 700×300 μm. Finely ground powders were placed on a non-conductive adhesive and mounted on an electrically grounded sample holder. High-resolution spectra of the Mn 2p, O 1s, Al 2p, Si 2p, and C 1s core lines were collected with a pass energy of 20 eV, a step size of 0.05 eV and a sweep time of 180 s. The precision of the measured binding energies was ±0.1eV. The charge neutralizer was used during collection of all spectra to counter the effects of differential charging. All XPS spectra were calibrated by setting the main C 1s feature resulting from adventitious C to 284.8 eV. The background from the high-resolution core-line XPS spectra was removed by fitting a Shirley-type background. All XPS spectra were fitted with component peaks having a combined Gaussian (70%) and Lorentzian (30%) line profile.

2.3 EELS data acquisition

EELS spectra were acquired using a FEI Titan 80-300 microscope (FEI Company, Eindhoven, The Netherlands), equipped with a monochromated S-FEG and a Gatan Tridiem 865 energy filter (GIF) (Gatan Inc., Pleasanton, CA). The microscope was operated at acceleration voltage

of 80keV, the energy resolution in monochromated mode was tuned to 0.08 eV FWHM at the zero-loss peak. The powder samples were finely ground and ultrasonicated in anhydrous ethanol for 5 minutes. A drop of each solution was deposited on a holey carbon TEM grid (SPI Supplies, West Chester, PA). The grids were heated to 160°C for 12 hours in a vacuum chamber to remove any hydrocarbon contamination present.

EELS spectra were acquired in scanning transmission electron microscopy (STEM) mode by sampling various areas of the sample. The beam current was set to approximately 100 pA, the exposure time per spectrum was 0.2 s, the GIF acceptance angle was 7 mrad and the energy dispersion was 0.1 eV/channel. The Mn-$L_{2,3}$ edge and O-K edge for all samples were recorded in one spectrum. To minimize beam damage to the sample, an area of several nm^2 was sampled with a total of a few hundred spectra each.

Processing of the EELS spectra was performed in Gatan Digital Micrograph 2.3. The pre-edge background was removed using a power-law function [30]. The Mn-$L_{2,3}$ and O-K edges were aligned in energy using the highest intensity feature of the Mn-L_3 edge and were normalized for baseline and intensity.

3 Results and Discussion

3.1 Powder X-ray Diffraction

Powder X-ray diffraction (XRD) patterns from the synthesized $MnAl_2O_4$, $MnSiO_3$, and Mn_2SiO_4 are presented in

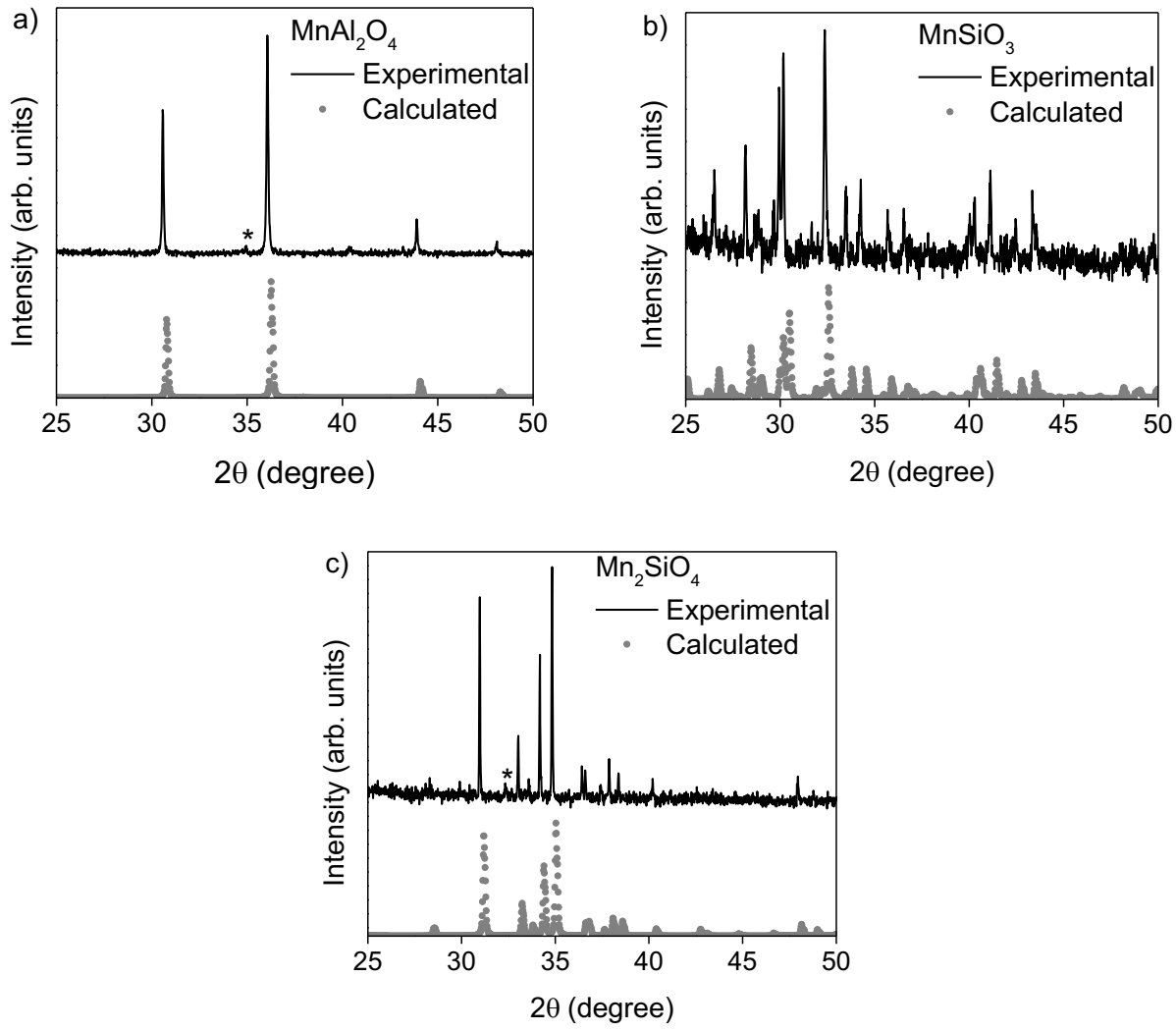

Figure 1 along with their calculated powder patterns [29]. Each diffraction pattern was found to contain either $MnAl_2O_4$ (cubic spinel; Fd-3m), $MnSiO_3$ (triclinic; C-1) or Mn_2SiO_4 (orthorhombic; Pbnm) as the dominant phase. The powder pattern for $MnAl_2O_4$ was observed to contain an impurity of MnO of less than a 5% whearas the diffraction pattern for $MnSiO_3$ indicated phase-purity and the diffraction pattern for Mn_2SiO_4 contained a minor impurity ($\leq$10%) of $MnSiO_3$. The materials studied were all considered to be highly crystalline owing to the flat background of the collected diffraction patterns, as any amorphous fractions present with

a concentration above the detection limit of the instrument (≤1 wt%) would show broad peaks in the 2θ of 20-40° (cf. references 40,41).

3.2 X-ray Photoelectron Spectroscopy Spectra

XPS is a very useful technique to investigate surface selective oxidation owing to its surface sensitivity and the sensitivity of the spectra to changes in composition and chemistry. In the present contribution, XPS has been used to identify differences in the core-line spectra from $MnAl_2O_4$, $MnSiO_3$, and Mn_2SiO_4. In particular, the XPS core-line spectra change in lineshape and shift in binding energy with changes in the chemical environment of the absorbing atom [21,31,32]. For example, the binding energy of a core-line spectrum generally shifts to a higher binding energy with increasing oxidation state as a result of reduced screening of the nuclear charge. Such a shift is referred to as a ground state effect; however, final-state effects (i.e. those that occur as a result of the excitation of the core-electron) can also shift the binding energy because of final-state relaxation [33]. Separating ground-state effects from final-state effects can make true assignment of the electronic structure of materials by analysis of XPS spectra alone difficult. In this current work, the focus was to identify differences in the spectra for these important standard materials and not to develop a complete understanding as to why shifts in binding energy were observed.

3.2.1 Mn 2p XPS spectra

The background subtracted Mn $2p_{3/2}$ XPS spectra for $MnAl_2O_4$, $MnSiO_3$, and Mn_2SiO_4 are presented in

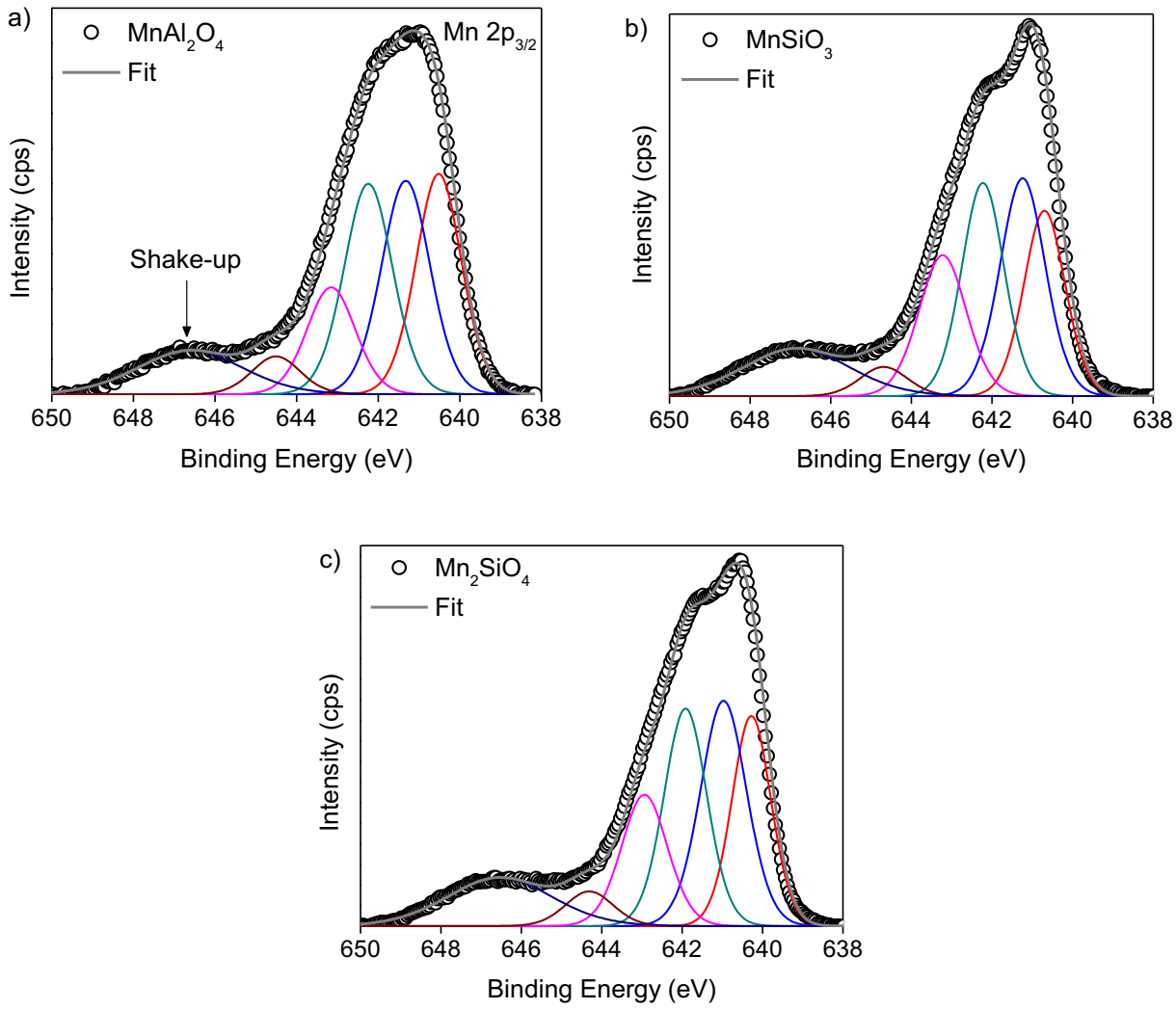

Figure 2. All three spectra are similar, but do show some differences. For example, each spectrum contains an intense signal resulting from direct excitation of a 2p electron that was broadened because of (final-state) multiplet spitting. The broad lineshape observed for these spectra is a common observation for 2p XPS spectra from first-row transition metals having a high-spin electron configuration [21,31,32]. A weak satellite peak can be observed at slightly higher binding energies, which is generally described as resulting from a ligand-to-metal charge transfer shake-up process [21,31,32].

As has been shown previously, both the lineshape and separation in energy between the core-line and shake-up satellite peak can be used to identify the oxidation state of transition metals [21,31]. In this case, all three Mn $2p_{3/2}$ spectra resemble those from Mn^{2+}, as would be expected based on the chemical formulae of the materials [21]. Examination of the spectra from the three materials show that the core-line peaks shift in energy and change slightly in lineshape as a function of the composition and structure of the materials. As was mentioned above, the spectra were broadened by multiplet splitting, which results from coupling between the unpaired 2p core-electron after excitation and unpaired 3d valence electrons [21]. It has been found that ligand effects can shift the energy of the final-states, and, therefore, change the lineshape of the spectra [21,32,34]. Here, it is proposed that the change in lineshape observed between $MnAl_2O_4$, $MnSiO_3$, and Mn_2SiO_4 can be ascribed to such effects.

Along with a change in lineshape, as can be seen from

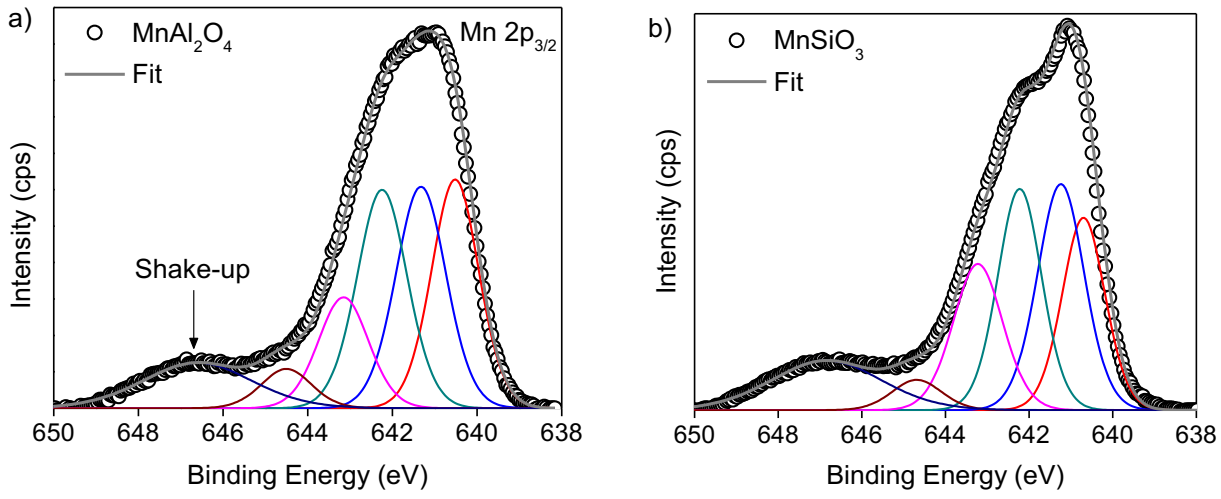

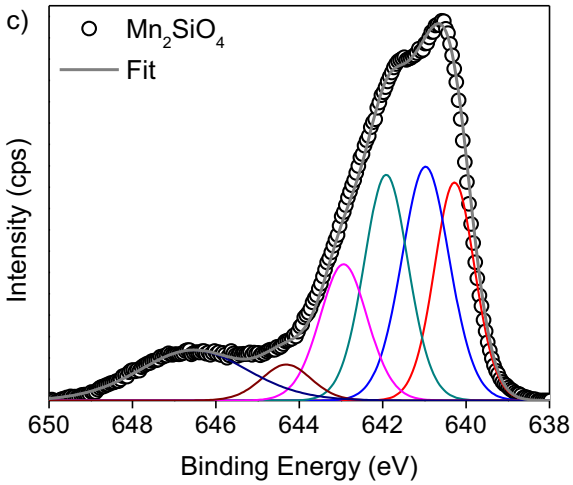

Figure 2, the binding energies of the Mn $2p_{3/2}$ core-line peak also changed as a function of composition, with $MnSiO_3$ having the highest binding energy, followed by $MnAl_2O_4$ and then Mn_2SiO_4. The spectra were fitted by a collection of multiplet component peaks using a previously developed procedure to accurately determine the Mn $2p_{3/2}$ binding energy for each material [21]. Based on this fitting procedure, the weighted average Mn $2p_{3/2}$ binding energy was determined to be 641.8 eV for $MnAl_2O_4$, 641.9 eV for $MnSiO_3$ and 641.5 eV for Mn_2SiO_4, where the calculation of the binding energy did not include the fitted shake-up satellite peak. These binding energy values are summarized in Table 2. Comparison of the Mn $2p_{3/2}$ binding energy for $MnAl_2O_4$ (641.8 eV) established in the present study agrees well with the previously established value of 641.6 eV [20] (Table 1).

It is interesting to note that Mn^{2+} is present almost exclusively in a tetrahedral site in $MnAl_2O_4$ while it is found in higher coordination sites in the other two materials investigated (Figure 3) [29,35]. It has been relatively recently found that a decrease in coordination number leads to a decrease in the binding energy of Fe $2p_{3/2}$ spectra for $SrFe_{1-x}Zn_xO_{3-\delta}$ [33]. Noting this, the Mn $2p_{3/2}$ binding energy from $MnAl_2O_4$ was located between that of Mn_2SiO_4 and $MnSiO_3$ (Table 2). The reason for these shifts in binding energy is not fully known, but may be related to variations

in the Mn-O bond covalency and Mn-O bond lengths between the materials, as the composition and structure also varied widely between the materials studied.

3.2.2 O 1s XPS spectra

The fitted O 1s XPS spectra for all the compounds studied are presented in

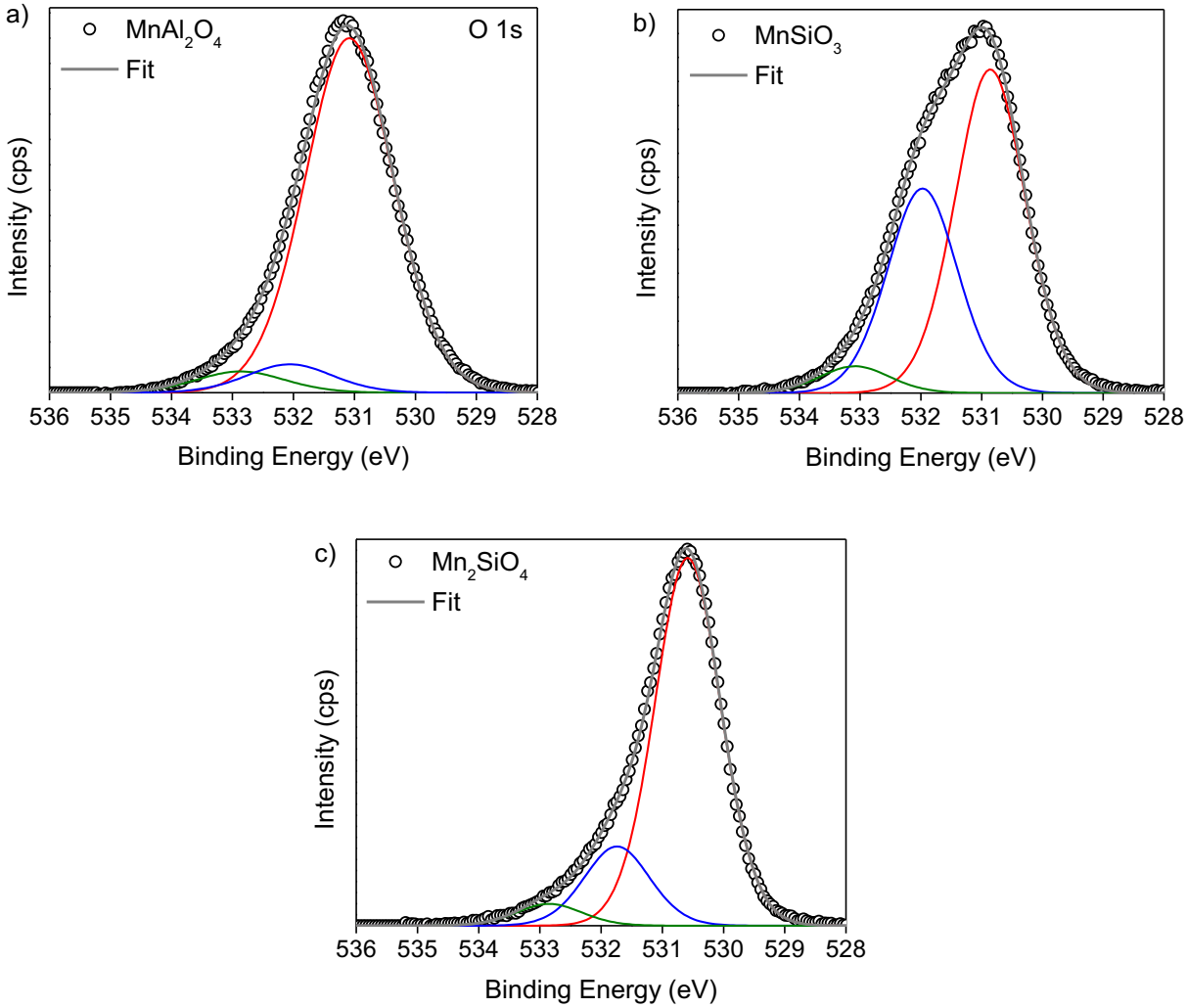

Figure 4. Similarly to the Mn $2p_{3/2}$ spectral observations, the O 1s binding energy for Mn_2SiO_4 was observed to be below that of $MnAl_2O_4$ and $MnSiO_3$. In the present case, the binding energy of the most intense, lowest energy feature in the spectra was determined to be 531.1 eV for $MnAl_2O_4$, 530.9 eV for $MnSiO_3$ and 530.6 eV for Mn_2SiO_4. It should be noted that the O 1s

binding energy reported here agrees well with the literature value reported in Table 1 (i.e. 531.3 eV [20]). However, contrary to the observations during analysis of the Mn $2p_{3/2}$ spectra, the O 1s peak maximum binding energy for $MnAl_2O_4$ was slightly above that of $MnSiO_3$. As can be easily observed in

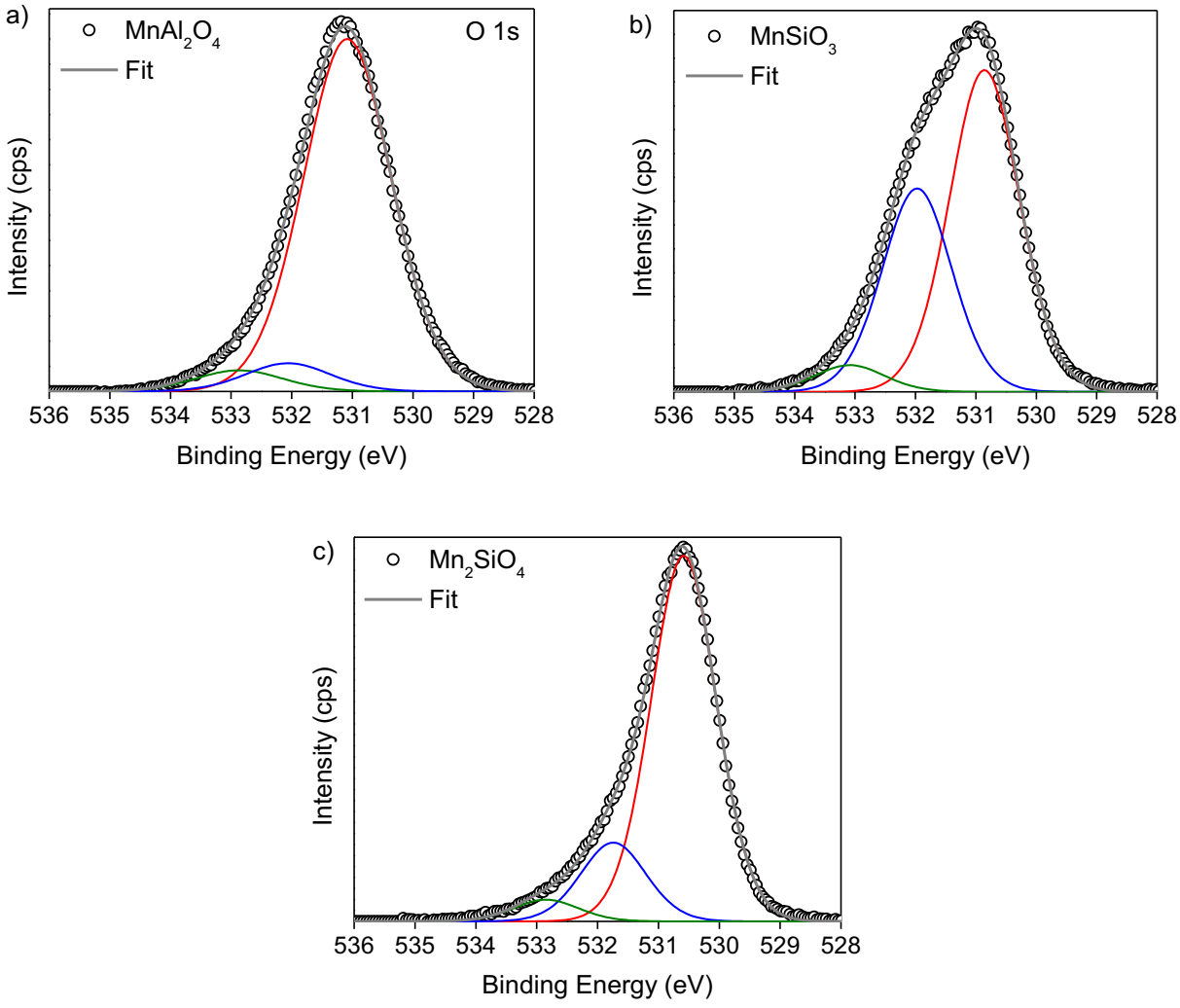

Figure 4, the O 1s lineshape from the materials changed considerably with composition. Such a change may result from the O ions being found in different chemical environments in the materials investigated. However, it should be noted that as the surfaces of the materials were not cleaned after being introduced into the vacuum chamber of the XPS instrument, it was likely that

the highest binding energy features (at least partially) resulted from adsorbed water and/or hydroxyl functional groups [36]. These binding energy data are also summarized in Table 2.

3.2.3 Al 2p and Si 2p XPS spectra

The fitted Al 2p and Si 2p XPS spectra for all experimental compounds are presented in Figure 5. All spectra were fitted by spin-orbit split $2p_{3/2}$ and $2p_{1/2}$ component peaks. Using this method, the Al $2p_{3/2}$ binding energy from $MnAl_2O_4$ was determined to be 74.3 eV while the 2p peak maximum energy was 74.5 eV (Figure 5(a)). This latter value is in good agreement with the previously reports Al 2p binding energy of 74.2 eV reported by Strohmeier and Hercules [20] (Table 1). Quite obviously, the presence of this XPS peak can be used to unambiguously distinguish $MnAl_2O_4$ from the Mn-silicates.

Using this same spin-orbit split peak fitting procedure, the Si $2p_{3/2}$ binding energy was determined to be 102.0 eV for $MnSiO_3$ and 101.4 eV for Mn_2SiO_4 whereas the Si 2p peak maximum energy was found to be 102.1 eV and 101.6 eV for $MnSiO_3$ and Mn_2SiO_4, respectively (Figure 5(b,c)). From this analysis, it can be said that the Si $2p_{3/2}$ and Si 2p binding energies for Mn_2SiO_4 were significantly less than those of $MnSiO_3$. These observations are important, as they provide the means by which the analyst can differentiate between the two Mn-silicates when studying the selective oxidation of advanced high strength steels using XPS. The Al and Si binding energy values derived in the present study are also summarized in Table 2.

3.3 Electron Energy Loss Spectroscopy

The Mn-$L_{2,3}$ energy loss near edge structure (ELNES) for $MnSiO_3$, $MnAl_2O_4$, and Mn_2SiO_4 are presented in Figure 6. It should be pointed out that the spectra have been aligned with respect to the highest intensity fine structure (FS) at 640 eV and do not allow direct comparison of the

absolute energy scale. Examination of the overall spectral weight of the Mn-L_3 edge towards low energy is consistent with the one found for MnO [37], and indicates an oxidation state close to 2+ for all the compounds investigated. This Mn valence was expected from a pure ionic description of the compounds, and is in agreement with the XPS results in the present study. Small differences were observed between the spectra. For example, at low energy, the FS at approximately 639 eV is clearly visible for Mn_2SiO_4, whereas it is much weaker for $MnSiO_3$ and $MnAl_2O_4$ (Figure 6). In addition, at approximately 642 eV, the FS is more clearly defined for $MnSiO_3$ and $MnAl_2O_4$ than it is for Mn_2SiO_4 (Figure 6). It can be argued that the highest intensity FS is actually located at higher energy for Mn_2SiO_4 than for $MnAl_2O_4$ and $MnSiO_3$, hence revealing the lowest energy shoulder and hindering the FS at 642 eV, which might be related to a slightly higher Mn oxidation state in Mn_2SiO_4 than in $MnAl_2O_4$ and $MnSiO_3$. Nevertheless, the noticeably higher intensity in the range 641.5-646 eV in the case of $MnSiO_3$ could also indicate a slightly higher oxidation state. Interpretation from calculations, such as the multiplet approach [38], would be necessary to discuss the structural origin of the spectral differences observed, but is beyond the scope of this study.

The O K-edge shows very distinct near edge structures for all the compounds, as shown in Figure 7. For example, the Mn_2SiO_4 spectrum (Figure 7, bottom curve) displays a shoulder at the edge onset just above 530 eV, two intense FSs and a shoulder at approximately 540 eV and finally a large structure from 550 eV corresponding to the first extended FS. This extended FS is also present in the case of the $MnSiO_3$ spectrum (Figure 7, top curve), but the near edge structures differ. In particular, in the case of the $MnSiO_3$ spectrum there is a low intensity pre-edge structure at approximately 526 eV which is absent in the two other spectra, a weak shoulder on the edge onset at approximately 530 eV and a relatively featureless and intense structure

between approximately 530 and 540 eV which is distinctly different from the Mn_2SiO_4 and $MnAl_2O_4$ spectra.

The O K-edge ELNES of $MnAl_2O_4$ (Figure 7, middle curve) is in agreement with the one reported in a recent investigation [39] and shows major differences versus the silicates. Several FSs are clearly visible: the FS at 530 eV, attributed to O *p* – Mn *p,d* hybridization [39], the highest intensity FS at approximately 537 eV, the shoulder at approximately 540 eV and the two FSs at approximately 543 and 545 eV. Furthermore, the extended fine structure between roughly 550 and 560 eV is more intense and has a narrower energy range than the similar FS observed for Mn_2SiO_4 and $MnSiO_3$. The differences observed in the O K-edge ELNES of these three compounds likely arise from the varying local environment around the O sites in these structures and can be discussed in terms of chemical bonding, but these determinations are beyond the scope of the present paper. However, the above results show that both the Mn $L_{2,3}$ and O K-edge EELS spectra have significant variances between the investigated compounds which can be used by the analyst to unambiguously identify these compounds in the TEM.

4 Conclusions

XPS and EELS spectra were acquired from $Mn_2Al_2O_4$, $MnSiO_3$ and Mn_2SiO_4 standards fabricated using the ceramic method with the objective of providing spectral data to aid in identifying these compounds when studying the selective oxidation of advanced high strength steels. It was determined that the Mn $2p_{3/2}$, O 1s, and Si 2p XPS spectra of Mn_2SiO_4 had a significantly lower binding energy versus those of $MnSiO_3$, with the difference in binding energy being greater than the precision of the instrument used in this study (± 0.1 eV). Noting this, however, the difference in Mn $2p_{3/2}$ binding energy between $MnAl_2O_4$ and $MnSiO_3$ was within

the precision of the instrument, making identification of these two materials by analysis of the Mn $2p_{3/2}$ binding energy alone difficult. However, the lineshape differences in the Mn $2p_{3/2}$ core-line peak spectra between the two materials can aid in identification. Further, the presence of the Al 2p or Si 2p XPS core-line peaks can be used to distinguish $MnAl_2O_4$ from $MnSiO_3$ in this case. Analysis of the EELS spectra for $Mn_2Al_2O_4$, $MnSiO_3$ and Mn_2SiO_4 revealed distinguishing features between the compounds in both the Mn $L_{2,3}$- and O K-edges. In particular, the O K-edge spectra for the three compounds were found to have very distinct fine structures, allowing the compounds to be easily distinguished from one another. Overall, the present contribution has provided both XPS and EELS spectral data which can be used to unambiguously distinguish $MnAl_2O_4$, $MnSiO_3$ and Mn_2SiO_4 when investigating the selective oxidation of advanced high strength steels in continuous galvanizing line process atmospheres.

5 Acknowledgements

The Natural Sciences and Engineering Research Council (NSERC) of Canada supported this work through a Discovery Grant awarded to APG. NSERC and U.S. Steel Canada are acknowledged for the financial support of JRM through the NSERC/U.S. Steel Industrial Research Chair in Advanced Coated Steels. The Canadian Foundation for Innovation (CFI) is thanked for providing funds to purchase the PANalytical Empyrean powder X-ray diffractometer used in this work. Dr. M. Biesinger from Surface Science Western, of Western University is thanked for collecting the XPS spectra reported in this study. The electron microscopy research described in this paper was performed at the Canadian Centre for Electron Microscopy at McMaster University, which is supported by NSERC and other government agencies.

6 References

1 E.M. Bellhouse, J.R McDermid, Selective Oxidation and Reactive Wetting During Hot-Dip Galvanizing of a 1.0 pct Al-0.5 pct Si TRIP-Assisted Steel, Metall. Mater. Trans. A 43A (2012) 2426-2441.

2 E.M. Bellhouse, J.R McDermid, Selective Oxidation and Reactive Wetting During Galvanizing of a CMnAl TRIP-Assisted Steel, Metall. Mater. Trans. A 42A (2011) 2753-2768.

3 E.M. Bellhouse, J.R McDermid, Selective Oxidation and Reactive Wetting of 1.0 Pct Si-0.5 Pct Al and 1.5 Pct Si TRIP-Assisted Steels, Metall. Mater. Trans. A 41A (2010) 1539-1553.

4 D.V. Edmonds, K. He, F.C. Rizzo, B.C. De Cooman, D.K. Matlock, J.G. Speer, Quenching and partitioning martensite – A novel steel heat treatment, Mater. Sci. Eng. A 438-440 (2006) 25-34.

5 H. Aydin, E. Essadiqi, I.-H. Jung and S. Yue, Development of 3rd generation AHSS with medium Mn content alloying compositions, Mater. Sci. Eng A 564 (2013) 501-508.

6 O. Grässel, L. Krüger, G. Frommeyer, L.W. Meyer, High strength Fe-Mn-(Al,Si) TRIP/TWIP steels development – properties – application, Int. J. Plasticity 16 (2000) 1391-1409.

7 Y. Suzuki, T. Yamashita, Y. Sugimoto, S. Fujita, S. Yamaguchi, Thermodynamic Analysis of Selective Oxidation Behavior of Si and Mn-added Steel during Recrystallization Annealing, ISIJ Int. 49 (2009) 564-573.

8 J. Mahieu, S. Claessens, B.C. De Cooman, F. Goodwin, Sufrace and Sub-surface Characterization of Si-, Al- and P-alloyed TRIP-aided Steels, Proc. 6th Int. Conf. on Zinc Alloyed Coated Steel Sheet, Galvatech'04, Chicago, IL, USA, Association for Iron and Steel Technology, (2004) 529-538.

9 P. Drillet, Z. Zermout, D. Bouleau, J. Mataigne, S. Claessens, Selective Oxidation of high Si, Mn and Al steel grade during Recrystallization Annealing, and steel/Zn reactivity, Proc. 6th Int. Conf. on Zinc Alloyed Coated Steel Sheet, Galvatech'04, Association for Iron and Steel Technology (2004) 1123-1134.

10 W. Mao, V.A. Lashgari, W. Melfo, W.G. Sloof, Effect of Cr on the Oxidation of Advanced High Strength Steels during Annealing Prior to Galvanizing, Proc. Galvatech 2015, Toronto, Canada, Association for Iron and Steel Technology (2015) 719-726.

11 Y. Suzuki, M. Miyata, N. Yoshimi, Effect of internal oxidation layer formed during annealing process on selective surface oxidation behavior and galvanizability of Si,Mn added steels, Proc. Galvatech 2015, Toronto, Canada, Association for Iron and Steel Technology (2015) 733-740.

12 L. Cho, E.J. Seo, B.C. De Cooman, Influence of Sn on the Selective Oxidation and Reactive Wetting of CMnSi TRIP Steel During Hot-Dip Galvanizing, Proc. Galvatech 2015, Toronto, Canada, Association for Iron and Steel Technology (2015) 762-768.

13 R. Kavitha, J.R. McDermid, On the in-situ aluminothermic reduction of manganese oxides in continuous galvanizing baths, Surf. Coat. Technol., 212 (2012) 152-158.

14 J. Staudte, J-M. Mataigne, F. Del Frate, D. Loison, S. Cremel, Optimizing the Manganese and Silicon Content for Hot Dip Galvanizing of 3rd Generation Advanced High Strength Steels, Proc. Galvatech 2013, Beijing, China, Chinese Society for Metals (2013) 133-138.

15 S. Alibeigi, J.R. McDermid, Effect of Bath Al on Interfacial Layer Formation for Continuous Galvanized Mn-Containing Steels, Proc. Galvatech 2013, Beijing, China, Chinese Society for Metals (2013) 171-176.

16 C. Hsu, K. Wang, L. Chang, D. Gan, T. Chen, K. Yang, Analyses of the Selective Oxides and Fe-Zn Interface of Annealed and Galvanized TRIP Steels Having Three Si/Mn Ratios, Proc. Galvatech 2013, Beijing, China, Chinese Society for Metals (2013) 87-91.

17 R. Sagl, A. Jarosik, D. Stifter, G. Angeli, The role of surface oxides on annealed high-strength steels in hot-dip galvanizing, Corr. Sci. 70 (2013) 268-275.

18 J. Finster, SiO_2 in 6:3 (Stishovite) and 4:2 Co-ordination – Characterization by Core Level Spectroscopy (XPS/XAES), Surf. Interface Anal. 12 (1988) 309-314.

19 F.J. Grunthaner, P.J. Grunthaner, R.P. Vasquez, B.F. Lewis, J. Maserjian, A. Madhukar, High-Resolution X-Ray Photoelectron Spectroscopy as a Probe of Local Atomic Structure: Application to Amorphous SiO_2 and the Si-SiO_2 Interface, Phys. Rev. Letters, 43 (1979) 1683-1686.

20 B.R. Strohmeier, D.M. Hercules, J. Phys. Chem. 88 (1984) 4922- 4929.

21 M.C. Biesinger, B.P. Payne, A.P. Grosvenor, L.W.M. Lau, A.R. Gerson, Resolving surface chemical states in XPS analysis of first row transition metals, oxides and hydroxides: Cr, Mn, Fe, Co and Ni, Appl. Surf. Sci. 257 (2011) 2717-2730.

22 A. Thompson, D. Attwood, E. Gullikson, M. Howells, K.-J. Kim, J. Kriz, J. Kortright, I. Lindau, P. Pianetta, A. Robinson, J. Scofield, J. Underwood, D. Vaughan, G. Williams, H. Winick, X-ray Data Booklet, 3rd ed., Lawrence Berkeley National Laboratory, Berkeley, 2009.

23 W. H. Casey, M.F. Hochella Jr., H.R. Westrich, The surface-chemistry of manganiferous silicate minerals as inferred from experiments on tephroite (Mn_2SiO_4), Geochimica et Cosmochimica Acta 57 (1993) 785-793.

24 X. Vanden Eynde, J.P.Servais, M. Lamberigts, Investigation into the surface selective oxidation of dual-phase steels by XPS, SAM and SIMS, Surf. Interface Anal. 35 (2003) 1004-1014.

25 T. Van De Putte, D. Loison, J. Penning, S. Claessens, Selective Oxidation of a CMnSi Steel during Heating to 1000°C: Reversible SiO_2 Oxidation, Metall. Mater. Trans. A 39A (2008) 2875-2884.

26 P. Casey, J. Bogan, J.G. Lozano, P.D. Nellist, G. Hughes, Chemical and structural investigation of the role of both Mn and Mn oxide in the formation of manganese silicate barrier layers on SiO_2, J. Appl. Physics 110 054507 (2011).

27 P. Casey, J. Bogan, B. Brennan, G. Hughes, Synchrotron radiation photoemission study of *in situ* manganese silicate formation on SiO_2 for barrier layer applications, Appl. Phys. Letters 98 113508 (2011).

28 J.H. Huang, E. Rosén, Determination of Gibbs free energies of formation for the silicates $MnSiO_3$, Mn_2SiO_4 and Mn_7SiO_{12} in the temperature range 1000 – 1350 K by solid state emf measurements, Phys. Chem. Minerals 21 (1994) 228-233.

29 FindIt Version 1.9.2 Inorganic Crystal Structure Database, Fachinformationszentrum Karlsruhe, Germany, 2013.

30 R.F. Egerton, Electron Energy-Loss Spectroscopy in the Electron Microscope. Plenum, New York, 1996.

31 A.P. Grosvenor, B.A. Kobe, M.C. Biesinger, N.S. McIntyre, Investigation of multiplet splitting of Fe 2p XPS spectra and bonding in iron compounds, Surf. Interface Anal 2004; 36 (2004) 1564-1574.

32 A.P. Grosvenor, M.C. Biesinger, R.St.C. Smart, N.S. McIntyre, New interpretations of XPS spectra of nickel metal and oxides, Surf. Sci. 600 (2006) 1771-1779.

33 M.W. Gaultois, A.P. Grosvenor. Coordination-induced shifts of absorption and binding energies in the $SrFe_{1-x}Zn_xO_{3-\delta}$ system J. Phys. Chem. C 114 (2010) 19822-19829.

34 P.S. Bagus, E.S. Ilton, J.R. Rustad, Ligand-field effects for the 3p photoelectron spectra of Cr_2O_3 Phys. Rev. B 69 205112 (2004).

35 U. Hålenius, F. Bosi, H. Skogby, Galaxite, $MnAl_2O_4$, a spectroscopic standard for tetrahedrally coordinated Mn^{2+} in oxygen-based mineral structures, Am. Mineral. 92 (2007) 1225-1231.

36 A.P. Grosvenor, B.A. Kobe, N.S. McIntyre, Studies of the oxidation of iron by water vapour using X-ray photoelectron spectroscopy and QUASES Surf. Sci. 572 (2004) 217-227.

37 J.H. Paterson, O.L. Krivanek, ELNES of 3d transition-metal oxides: II. Variations with oxidation state and crystal structure. Ultramicroscopy, 32(4) (1990) 319-325.

38 F.M.F. De Groot, Multiplet effects in X-ray spectroscopy. Coord. Chem. Rev. 249 (2005) 31-63.

39 S. Nyquist, U. Hålenius, An EELS study of near edge structures of the oxygen K-edge in spinels, Phys. Chem. Minerals 41(4) (2014) 255-265.

40 Y. N. Ko, S. B. Park, S. H. Choi, Y. C. Kang, One-pot synthesis of manganese oxide-carbon composite microspheres with three dimensional channels for Li-ion batteries, Sci. Rep. 4 (2014) 5751.

41 P. Wang, M. Du, M. Zhang, H. Zhu, S. Bao, The preparation of tubular heterostructures based on titanium dioxide and silica nanotubes and their photocatalytic activity, Dalton Trans. 43 (2015) 1846 – 1853.

List of Figures

List of Tables

Table 1: XPS binding energies for Mn_2SiO_4 and $MnAl_2O_4$ available in the literature.

Compound	Al 2p	O 1s	Mn $2p_{3/2}$	Mn $2p_{1/2}$	Si 2p	Reference
$MnAl_2O_4$	74.2	531.3	641.6	653.4		[20]
Mn_2SiO_4					~102.5	[23]

Table 2: Summary of experimentally determined XPS binding energies (eV).

Compound	Al 2p (Al $2p_{3/2}$)	O 1s	Mn $2p_{3/2}$	Si 2p (Si $2p_{3/2}$)
$MnAl_2O_4$	74.5 (74.3)	531.1	641.8	--
$MnSiO_3$	--	530.9	641.9	102.1 (102.0)
Mn_2SiO_4	--	530.6	641.5	101.6 (101.4)

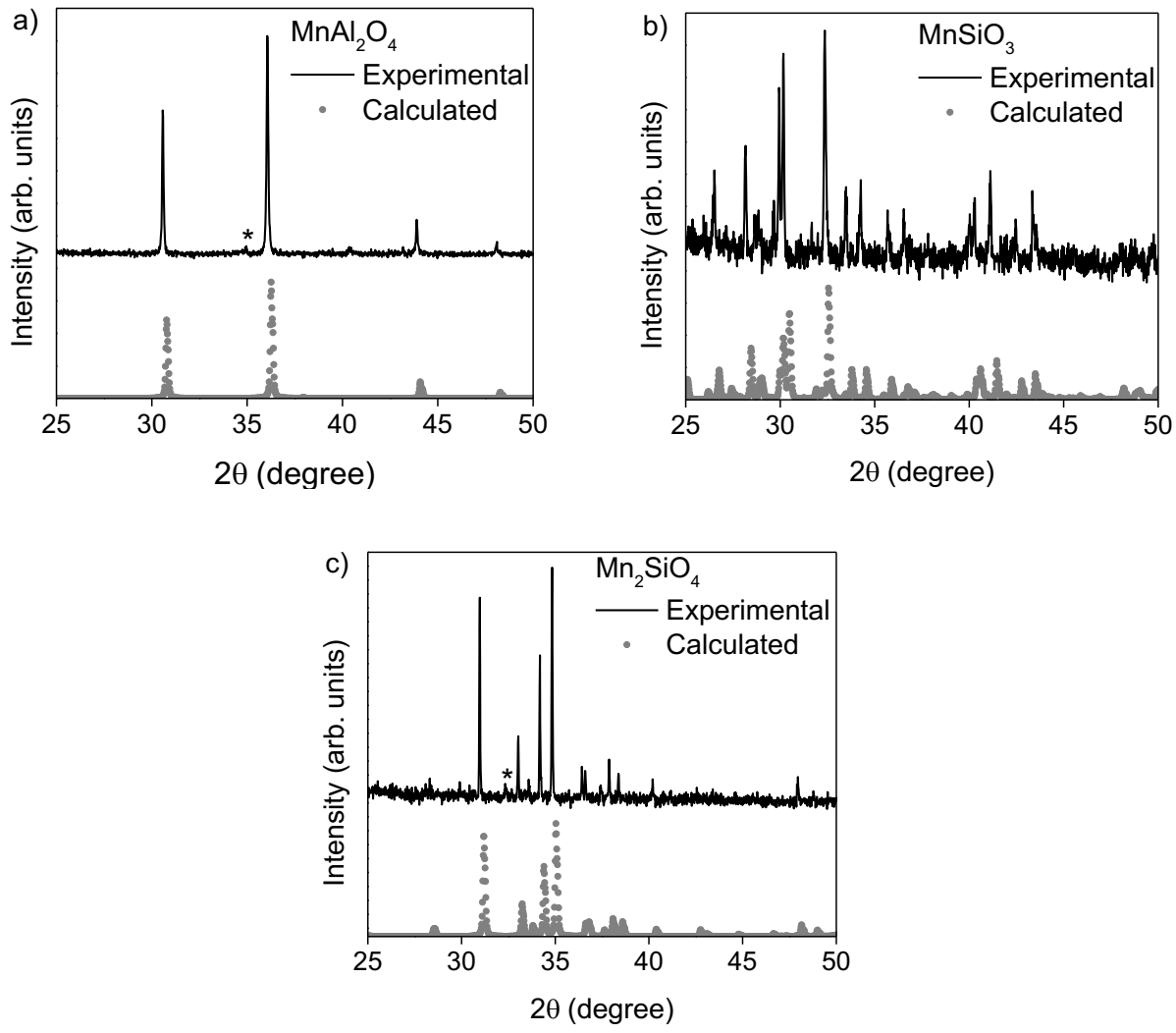

Figure 1: Powder X-ray diffraction patterns from (a) $MnAl_2O_4$, (b) $MnSiO_3$, and (c) Mn_2SiO_4 collected using a Cu $K_{\alpha 1}$ X-ray source. The collected diffraction patterns are compared to the calculated diffraction patterns determined using the known structures of the materials [29]. The major peaks from the impurity phases are marked with an asterisk in the powder XRD patterns.

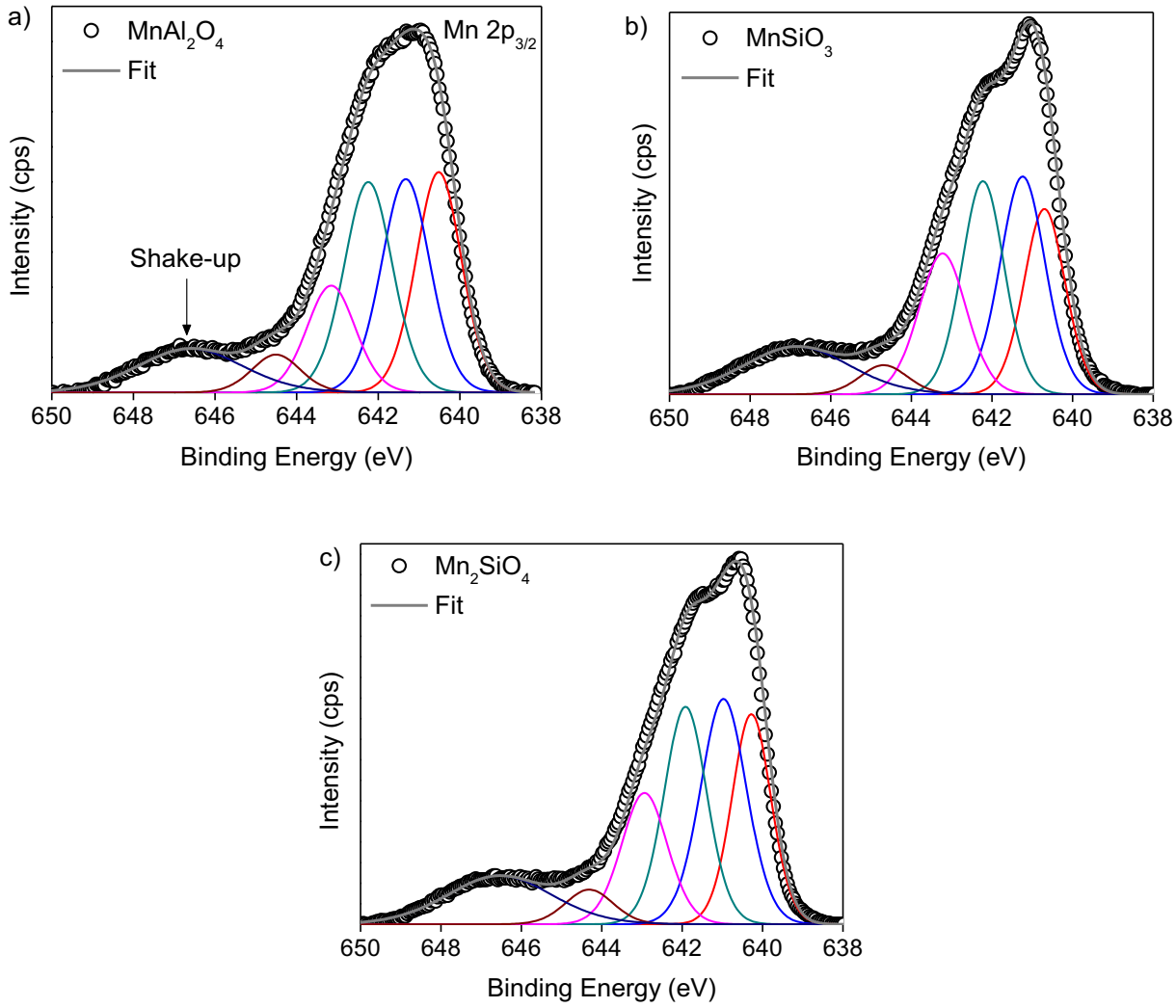

Figure 2: Background subtracted Mn $2p_{3/2}$ high resolution XPS spectra from (a) $MnAl_2O_4$, (b) $MnSiO_3$, and (c) Mn_2SiO_4. The background was removed using a Shirley-type background and the spectra were fitted using multiplet peaks and a shake-up satellite peak using the method described in [21]. The resulting fit is indicated by a grey line.

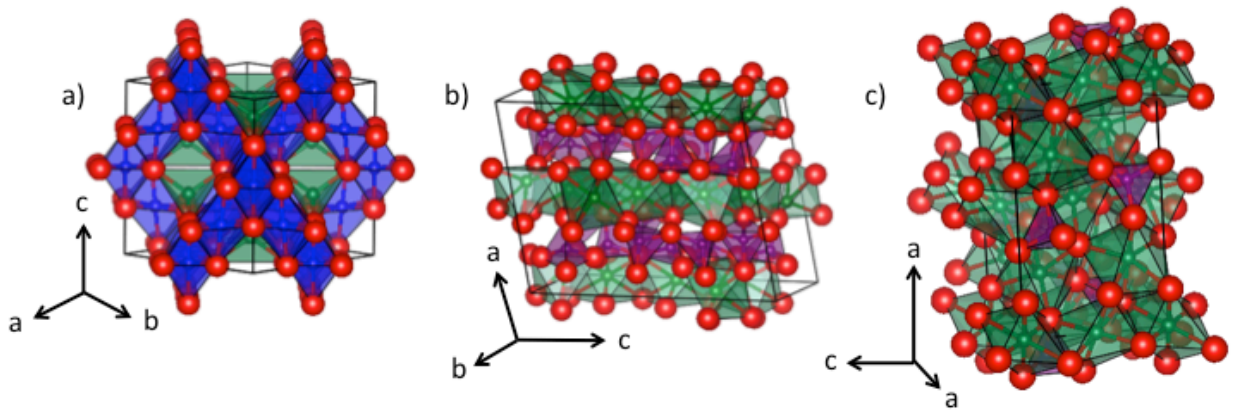

Figure 3: Crystal structures of (a) $MnAl_2O_4$, (b) $MnSiO_3$, and (c) Mn_2SiO_4. Mn-O polyhedra are shown in green, Si-O polyhedral are shown in purple, and Al-O polyhedral are presented in blue. Mn is 4-coordinate in $MnAl_2O_4$, whereas distorted 6- and 7-coordinate Mn ions are present in $MnSiO_3$, while Mn occupies distorted octahedral environments in Mn_2SiO_4.

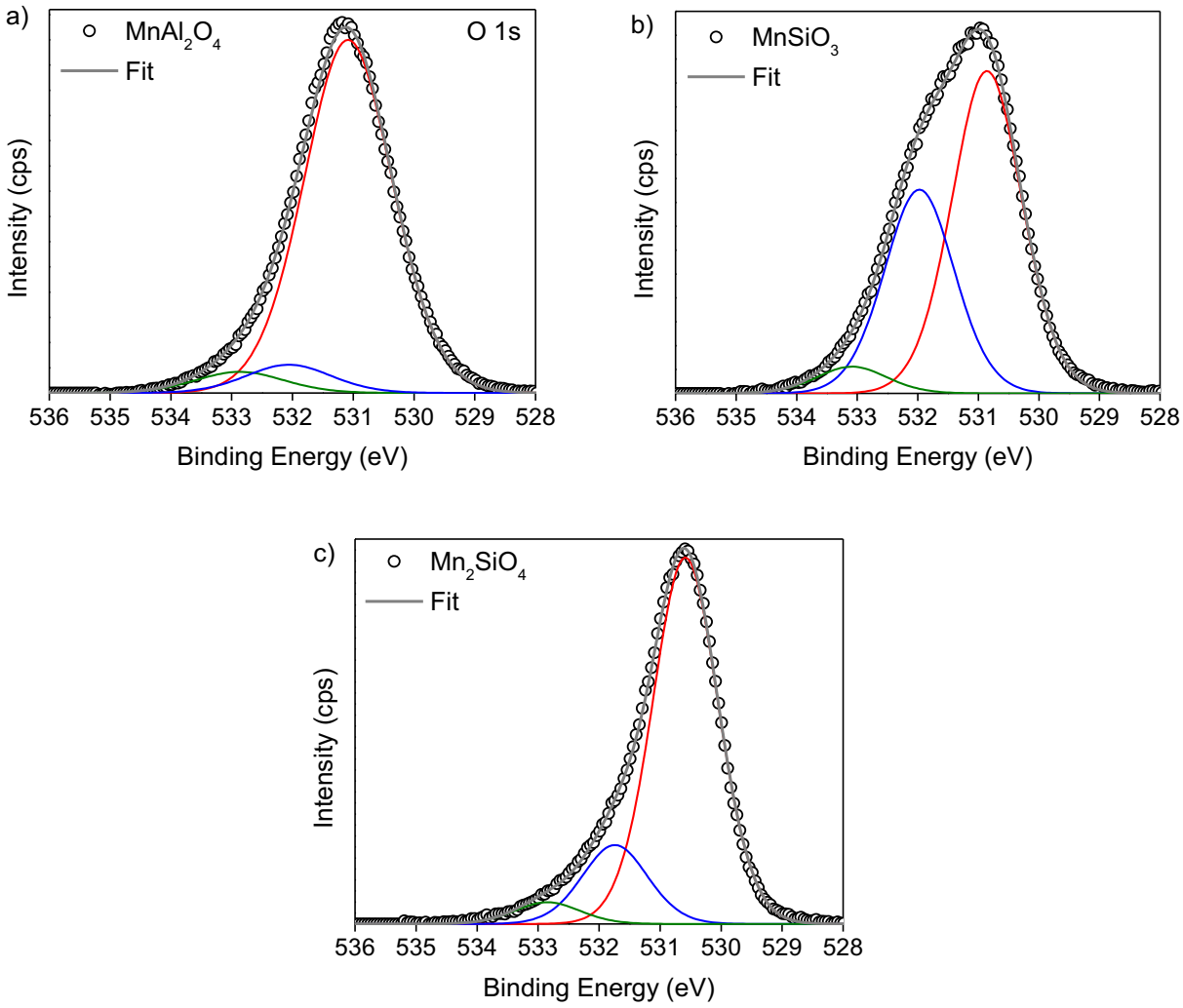

Figure 4: Background subtracted O 1s high resolution XPS spectra from (a) $MnAl_2O_4$, (b) $MnSiO_3$, and (c) Mn_2SiO_4. The spectra were fitted by three component peaks to adequately reproduce each spectrum. The lowest energy peak represents O ions bound to Mn/Al/Si while the highest energy peaks likely represents adsorbed water and hydroxide functional groups [36].

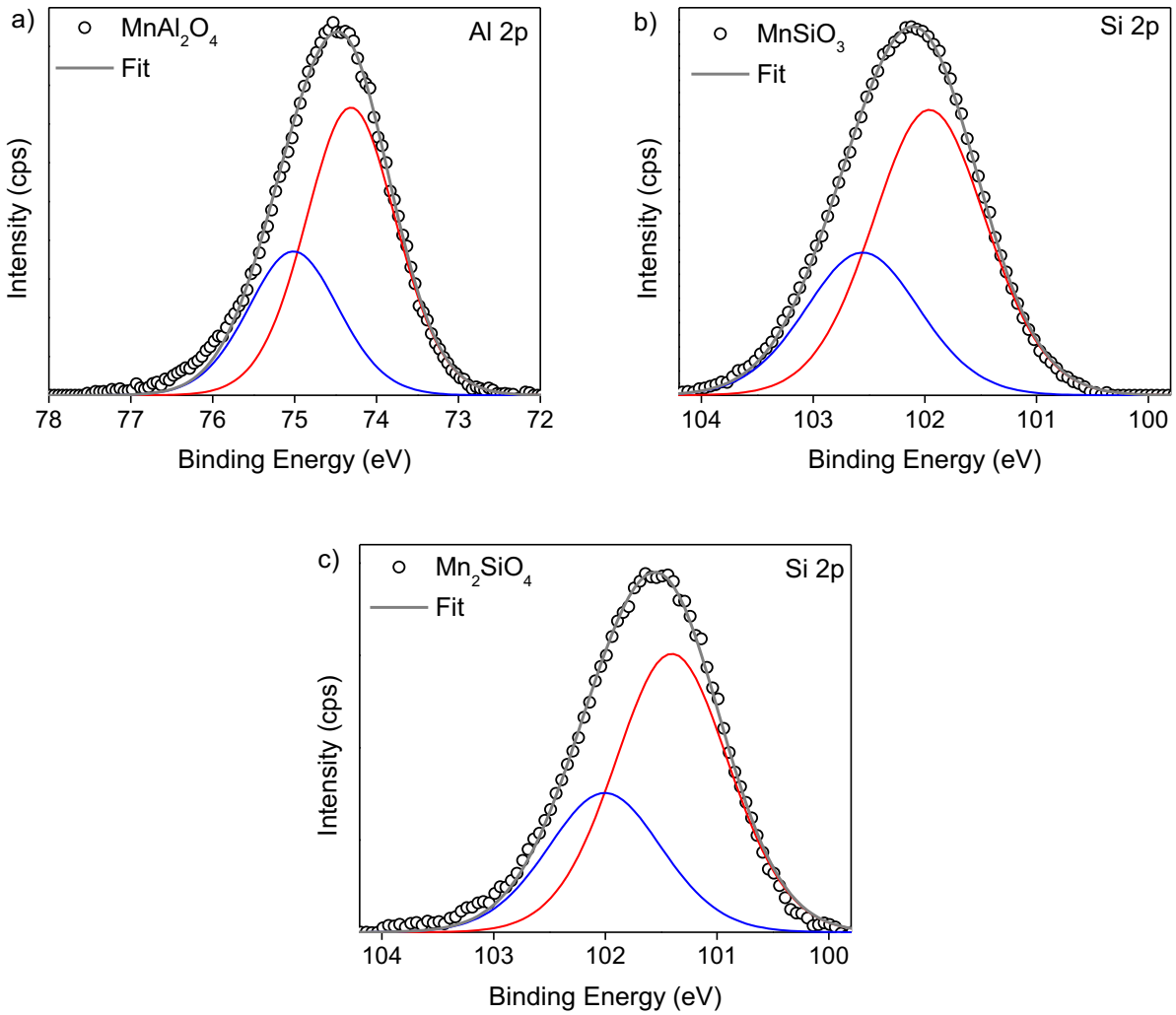

Figure 5: Background subtracted high resolution Al 2p XPS spectrum from (a) $MnAl_2O_4$ and high resolution Si 2p XPS spectra from (b) $MnSiO_3$ and (c) Mn_2SiO_4. Each spectrum has been fitted by a set of spin-orbit split $2p_{3/2}$ (low energy) and $2p_{1/2}$ (high energy) peaks having a 2:1 intensity ratio.

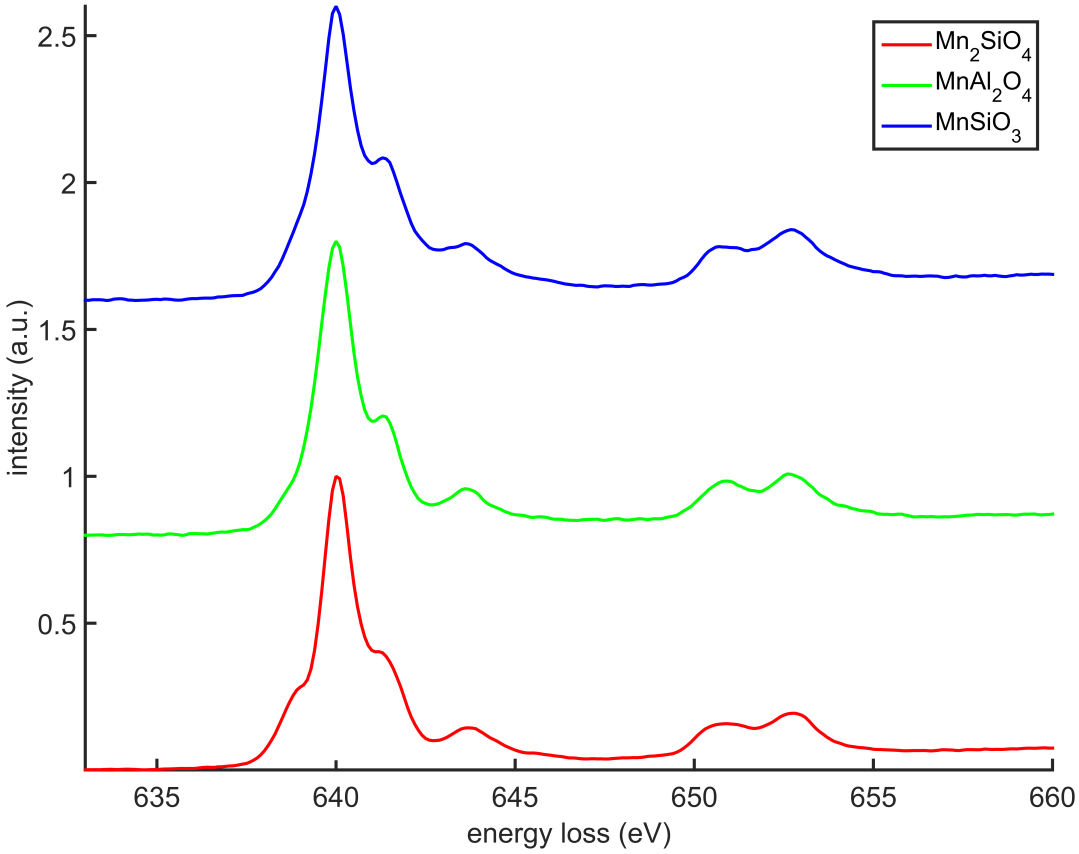

Figure 6: Mn-$L_{2,3}$ edge electron energy loss spectra. The spectra were aligned to the most intense fine structure of the L_3 edge at approximately 640 eV. The spectra were normalized to have an equal intensity of the L_3 edge and were offset for clarity.

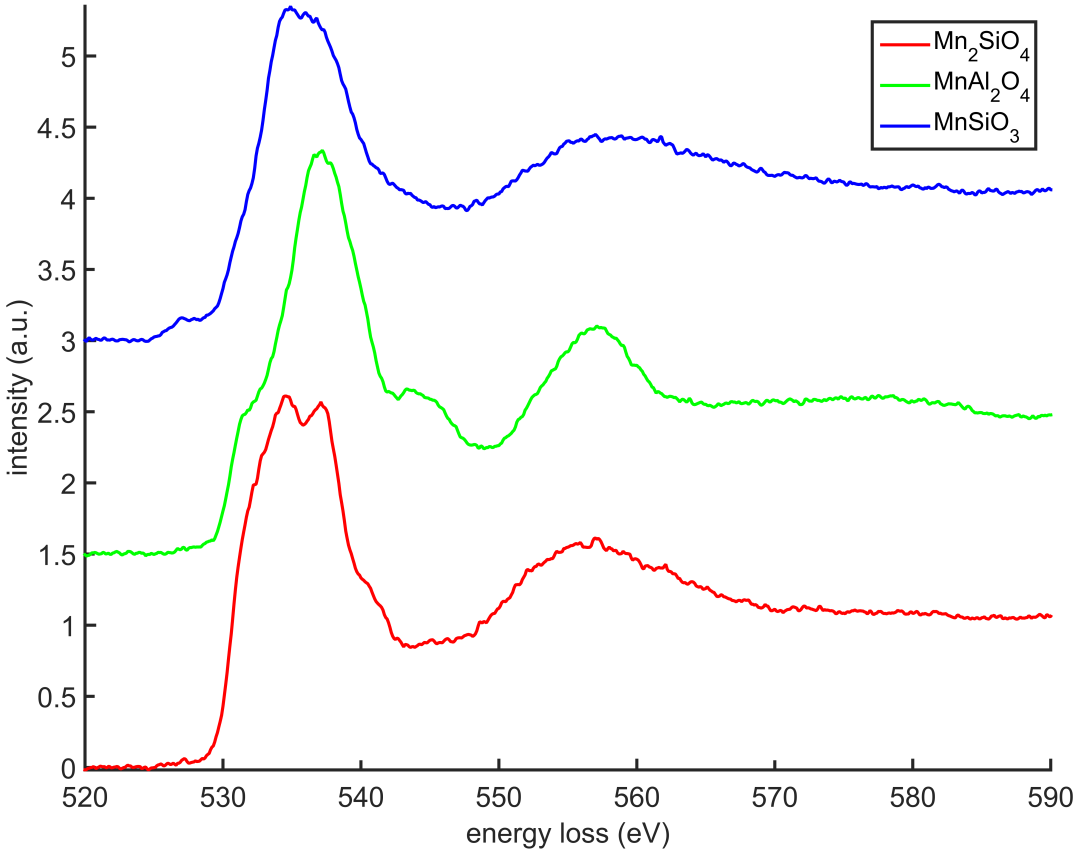

Figure 7: O-K edge electron energy loss spectra. The alignment and normalization of the spectra were performed with respect to the most intense fine structure of the Mn-L_3 edge (Figure 6) and the spectra were offset for clarity.